



Solid state synthesis of cadmium doped ZnS with excellent photocatalytic activity and enhanced visible light emission

S. Suganya¹ · M. Jothibas¹ · S. Johnson Jeyakumar¹

Received: 10 November 2018 / Accepted: 11 March 2019 / Published online: 18 March 2019
© Springer Science+Business Media, LLC, part of Springer Nature 2019

Abstract

Pure and Cd-doped ZnS nanoparticles were synthesized by inexpensive solid state reaction method at different percentages (0.5, 1.0, 1.5 and 2.0 wt.%). The structural, functional, optical, morphological and photocatalytic properties were characterized by using X-ray diffraction analysis, Fourier transform of infrared (FT-IR) spectroscopy, UV–Vis spectroscopy, photoluminescence (PL) spectroscopy and scanning electron microscopy (SEM) were done using energy dispersive X-ray analysis. In XRD pattern crystalline size, microstrain, dislocation density and lattice constant were found and they confirmed the crystalline nature with cubic structure. SEM and TEM exposed the great quantity of sphere-shaped particles and the elements Zn, S and Cd were identified from EDS. The photo-degradation rate was sturdily inclined by activation of ZnS photocatalyst with photon and creation of hydroxyl radicals. This suggested that Cd doping enhanced catalytic activity in the ZnS lattice.

1 Introduction

In modern years, nanostructure materials have become as a main subject for the intensive research because of their potential application in the fabrication of nano devices. Due to their large exterior volume percentage and quantum confinement effects, the electronic, magnetic and optical properties of nanomaterials get appreciably distorted compare to their bulk counterparts [1]. Mostly, one dimensional nano structures have been prepared from II to VI and semiconductor group is prepared from III to V group semiconductor. Among these ZnS is a typical II–VI semiconductor composite with band gap energy of 3.6 eV and a small Bohr radius (2.4 nm). Cadmium has tremendous spacious bandgap. It is semiconductor substance with fascinating properties such as, photoluminescent phenomenon [2, 3], which is composed of exceptional applicant for exploring the intrinsic recombination progression intense excitonic systems. Environment is polluted by organic contamination, which comes from toxic waste water and has attracted more attention in modern years [4–6]. Safe and clean technologies are now required to reduce pollution [7–9]. To resolve the above problem, semiconductor photocatalyst like Cd doped ZnS which is

clean, easy to operate and with high efficiency is used in this work. The sunlight and the organic substance like methyl orange dye are used along with Cd doped ZnS photocatalysts to purify the contaminated water [10–13]. Many techniques such as, chemical vapour deposition [14] wet chemical route [15] co-precipitation [16] solvothermal synthesis [17] hydrothermal process [18] thermal decomposition method [19] radio frequency magnetron sputtering technique [20] and solid state reaction method are used to prepare ZnS nanoparticles. Solid state reaction method is cheap, non-toxic and eco-friendly. So this method is used in the present work for the production of ZnS and Cd -doped ZnS nanoparticles at different concentrations (0.5, 1.0, 1.5 and 2.0 wt.%) and the photocatalytic property is studied for the prepared materials.

2 Experimental details

2.1 Solid state synthesis of Cd-doped ZnS nanoparticles

In this study, Zinc acetate dehydrate, thiourea and cadmium acetate of high purity were used to form Cd-doped ZnS nanoparticles. For typical synthesis, Zinc acetate dehydrates and thiourea were grounded by using agate mortar. To achieve Cd doping, different concentrations (0.5, 1.0, 1.5 and 2.0 wt.%) were added to the mixed powder and ground thoroughly. Finally, mixed powder was heated in a muffle

✉ M. Jothibas
jothibas1980@gmail.com

¹ PG& Research Department of Physics, T.B.M.L. College, Porayar, Tamilnadu 609307, India

furnace at about 4000C for 4 h. Wang and Hang used this method [21] to prepare Cd-doped ZnS nanoparticles.

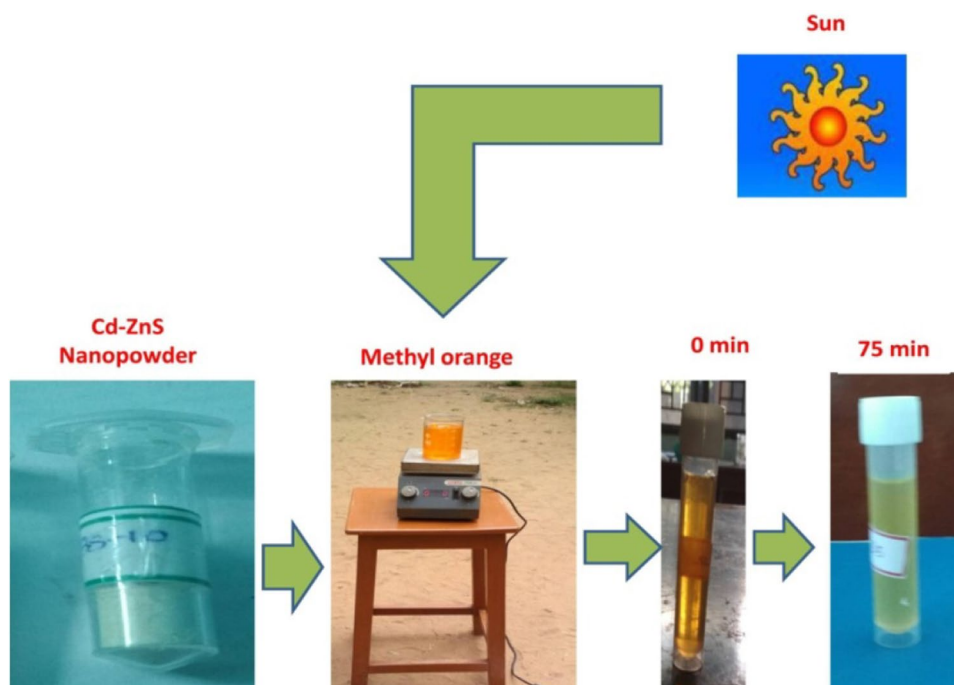
2.2 Characterization tools

The crystalline phase purity of ZnS was analyzed by X-ray diffraction analysis using SHIMADZU 6000X-ray diffractometer with $\text{CuK}\alpha$ radiation ($\lambda = 1.506 \text{ \AA}$) at room temperature. The chemical structure was examined by SHIMADZU Fourier transform infrared (FTIR) spectrometer in which the IR in spectra were recorded by diluting the minced powders in KBr and at the wavelength between 4000 and 400 cm^{-1} . Optical absorption spectra were recorded in the range 200–1200 nm using JASCO v-670 spectrophotometer. The photoluminescence (PL) behavior was pre-meditated at room temperature by Plorolog 3-HORIBA JOBIN YVON with an excitation wavelength of 325 nm. The morphology of the samples was characterized by SEM (Hitachi S-4500 SEM Machine) and HRTEM analysis (TECNAI F20).



Fig. 1 Structure of methyl orange

Fig. 2 Photo catalyst diagram of Methyl orange



2.3 Photocatalytic activity

Methyl Orange (99.5% purity) and the natural reagents are purchased from Sigma-Aldrich. The structure of methyl orange is shown in Fig. 1. To assess the photocatalytic activity of pure and Cd doped ZnS nanoparticles, photodegradation of MO dye under sunshine irradiation was carried out. The photocatalytic experiment was carried out on sunny day. The stock solution of dye was prepared by dissolving 10 mg of MO dye in 500 ml of water. Before illumination, the suspension of Pure and Cd doped ZnS nanoparticles (0.06 g Cd doped ZnS in 100 ml dye solution) were stirred in dye, was stirred in dark for 60 min in the dark to equilibrate the solution. After equilibration of solution, the suspension was illuminated in indigenous sunlight reactor for 75 min, till the dark orange color was changed to colorless, and it is shown in Fig. 2.

3 Results and discussion

3.1 Crystallographic analysis

Powder X-ray diffraction patterns of pure and Cd-doped ZnS nanoparticles are synthesized at different percentages (0.5, 1.0, 1.5 and 2.0 wt.%) with Miller indices (hkl) showing the crystal family of planes for each diffraction peaks and it is depicted in Fig. 3. The intense diffraction peaks appear at about 2θ of 28.69° , 47.62° , 56.59° are corresponding with

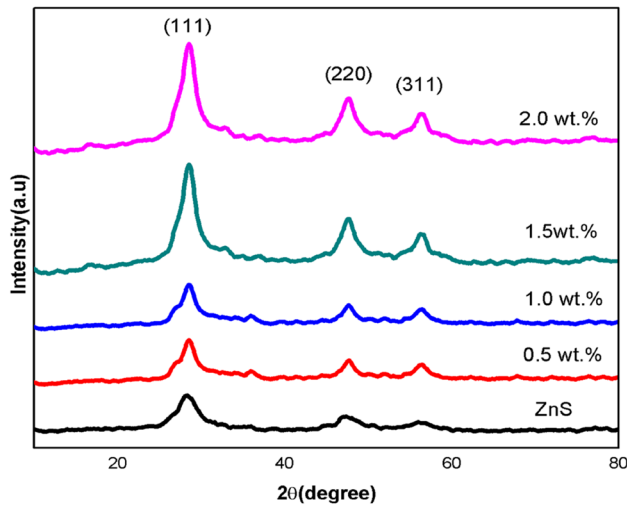


Fig. 3 XRD patterns of pure and Cd doped ZnS nanoparticles

those from (111), (220) and (311) orientations, respectively. This spectra show a strong preferred orientation along (111) direction and it has comparatively low intensity reflections corresponding to (220) and (311) planes, which was in good agreement with the standard JCPDS (05-0566) values of ZnS compound.

The XRD peaks were extensively broadened because of the small crystal size [22]. The crystallite size had been inferred from 2θ and the full width half maximum (FWHM) of the diffraction peak on the basis of Debye-Scherrer's relation

$$D = \frac{K\lambda}{\beta \cos \theta}$$

Table 1 Structural parameter of Pure and Cd doped ZnS nanoparticles

Sample wt. %	2θ (degree)	D space	FWHM	$\cos\theta$	Crystalsize D (nm)	Average crystal size
ZnS	28.3166	3.1466	2.7330	0.9696	3.1977	3.68
	47.5375	1.9112	2.6750	0.9151	3.3879	
	56.4000	1.6300	2.1000	0.8813	4.4814	
Cd(0.5)	28.4625	3.1333	1.9250	0.9693	4.4450	5.39
	46.6000	1.9083	1.5500	0.9149	5.8483	
	56.3000	1.6327	1.6000	0.8813	5.8791	
Cd(1.0)	28.6250	3.2264	2.7500	0.9690	3.1126	4.04
	46.5250	1.9504	1.6500	0.9187	4.6478	
	56.0750	1.6661	2.1500	0.8867	4.3706	
Cd(1.5)	28.4053	3.1395	2.2393	0.9694	3.8206	4.26
	47.5550	1.9105	2.1900	0.9149	4.1385	
	56.2750	1.6334	1.9500	0.8810	4.8223	
Cd(2.0)	28.5000	3.1293	1.5000	0.9692	5.7048	6.68
	47.6033	1.9087	1.1730	0.9149	7.7261	
	56.0750	1.6387	1.5500	0.8826	6.6026	

where D is the average crystallite size (\AA), K is the shape factor (0.9), λ is the wavelength of X-ray (1.5406 \AA) CuK α radiation, θ is the bragg angle and β is the Full width half maximum. The lattice constants $a=b=c$ is calculated using the subsequent formula used for cubic (fcc) systems [23].

$$d = \frac{a}{\sqrt{h^2 + k^2 + l^2}}$$

where d is the lattice spacing, a , b and c are the lattice constants, h , k , and l are the Miller indices, θ is the angle of corresponding peak and λ is the wavelength of X-ray used ($\lambda = 1.5406 \text{ \AA}$) [24]. The structural parameters are calculated from the following equations [25].

$$\text{Microstrain, } \epsilon = \frac{\beta \cos \theta}{4}$$

$$\text{Dislocation density, } \delta = \frac{1}{D^2} \text{ lines/m}^2$$

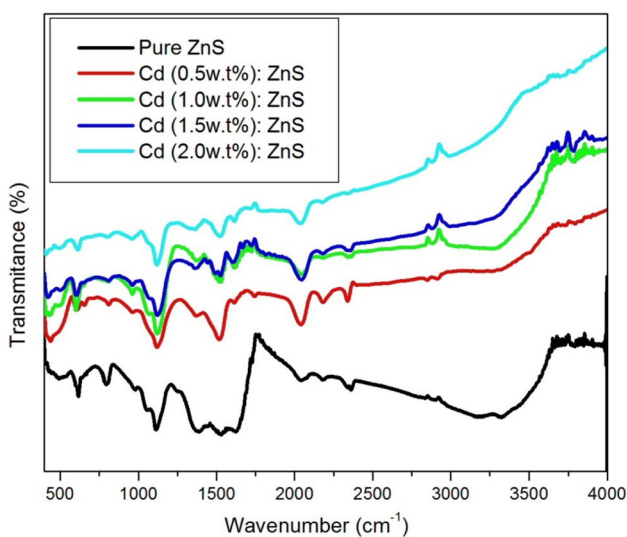
The dislocation density (δ) gradually decreases from $10.32211 \times 10^{14} \text{ lines/m}^2$ to $3.0726 \times 10^{14} \text{ lines/m}^2$ as doping concentrations increases upto 0.5 to 2.0 wt.%. Microstrain (ϵ) of the decreases from value to $0.1132 \times 10^{-3} \text{ m}$ $0.0063 \times 10^{-3} \text{ m}$. The average lattice constant is from 5.4221 to 5.5435 \AA and it is shown in Tables (1, 2). This may be due to the improvement of crystallinity as well as the high orientation along (111) direction (Figure. 3). This type of change in δ and ϵ might be due to the recrystallization process in the polycrystalline nature [26].

Table 2 Structural parameter of Pure and Cd doped ZnS nanoparticles

Sample wt. %	Dislocation density $\delta(10^{14})$	Micro-strain $\epsilon(x10^{-3})$	Lattice constant (Å)	Average lattice constant (Å)
ZnS	9.7796	0.1132	5.4545	5.4221
	8.7122	0.0106	5.4056	
	4.9122	0.0080	5.4063	
Cd (0.5)	10.3211	0.0116	5.4271	5.4137
	4.6290	0.0077	5.3989	
	5.2349	0.0082	5.4152	
Cd (1.0)	7.5703	0.0099	5.5883	5.5435
	3.3403	0.0066	5.5165	
	2.8574	0.0019	5.5259	
Cd (1.5)	6.8506	0.0094	5.4378	5.4196
	5.8386	0.0087	5.4037	
	4.2983	0.0075	5.4174	
Cd (2.0)	3.0726	0.0063	5.4210	5.4190
	1.6752	0.0046	5.3996	
	2.7208	0.0059	5.4365	

3.2 FT-IR spectroscopy

The presence of different chemical and functional groups of Pure and Cd doped ZnS nanoparticles are supported by FT-IR spectra (Fig. 4). Several peaks are observed at 3257, 2355, 2181, 2060, 1393, 1116, 798 and 614 cm^{-1} for the pure ZnS. The broad absorption peaks at 3257 cm^{-1} are attributed at O–H stretching. 2355, 2181, and 2060 cm^{-1} are due to C=O stretching. The peaks appearing at 798 and 614 cm^{-1} are attributed to Zn–S vibration and are

**Fig. 4** FTIR spectra of Pure and Cd doped ZnS nanoparticles at different doping concentrations

characteristic of cubic ZnS [27]. The 0.5% of cadmium doped ZnS peaks appear at 2346, 2184, 2048, 1516, 1126, 809, 644 and 583 cm^{-1} . 1.0% at 2920, 2878, 2060, 1618, 1525, 1362, 1116 and 583 cm^{-1} , 1.5% at 2930, 2848, 2325, 2048, 1628, 1383 and 1116 cm^{-1} . 2.0% at 2930, 2858, 2039, 1525, 1126, 614 and 400 cm^{-1} (Table 3). The intensity of the IR peaks for Cd doped ZnS nanoparticles is higher than that of pure nanoparticles, which stipulate the similar formation of particles.

3.3 Optical study

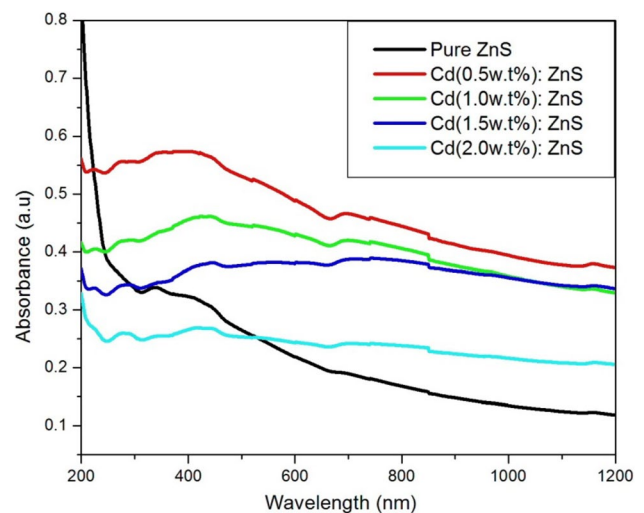
The absorption spectra of the pure and Cd-doped ZnS nanoparticles is illustrated in (Fig. 5). The absorption edge around 418, 394, 415, 425, 431 nm is due to Pure and Cd doped Zinc sulfide. The absorption co-efficient is calculated using the formula,

$$\alpha = 2.303A/l$$

where A is the absorbance and l is the path length. The value of optical band gap is determined from the absorption spectra with the Tauc relation,

$$\alpha h\nu = A(h\nu - E_g)^n$$

where α is the absorption coefficient, A is having separate value for different transitions, $h\nu$ is the photon energy and E_g is the band gap energy. The values of n depend upon the nature of transition. The values n of direct changes in the allowed are 1/2, 2, 3/2 and 3 respectively. Figure 6 ($\alpha h\nu$)² versus $h\nu$ shows the curves of Cd doped ZnS nanoparticles in different concentrations. The diagonal portions of the map are comparable to x-axis. The energy band spaces measured from these layers are shown in Table 4. E_g values from this table are 3.45 to 3.77 eV for Cd doped ZnS nanoparticles at

**Fig. 5** UV–Vis spectra of pure and Cd doped ZnS nanoparticles

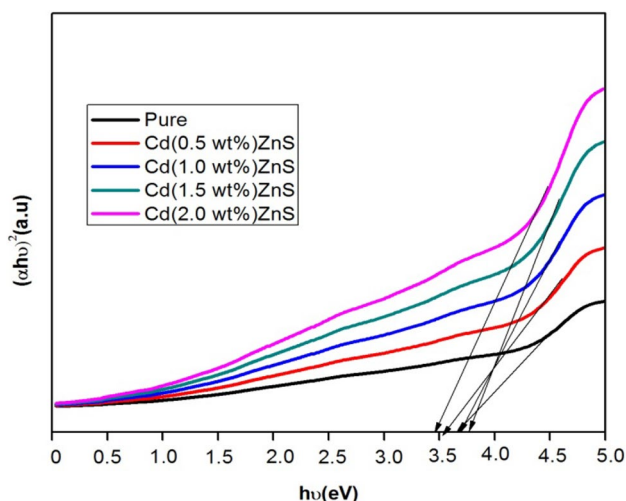


Fig. 6 Band gap spectra of pure and Cd doped ZnS nanoparticles

different concentrations. The pure ZnS nanoparticles reveals a superior bandgap energy of 3.66 eV. Cd-doped ZnS nanoparticles bandgap energy varies between 3.45 and 3.77 eV. A decrease in bandgap is noticed in the Cd doped ZnS, when compared with pure ZnS. The red shift in the bandgap is due to the replacement of Zn^{2+} ions in ZnS lattice by Cd^{2+} ions, while doping [28]. After the electronic absorption process, electrons remain in the maximum energy state and again they are transmuted to minimum energy state at the same point in the Brillouin zone [29, 30].

3.4 Photoluminescence spectroscopy

The PL spectra were recorded for the present doped nano material; ZnS which was shown in the Fig. 7 in which the peaks related to the doping concentration from 0.5 to 2.0 Wt.%. In this case, the broad peak was observed in the range of 420–550 nm for pure ZnS. At 0.5 Wt.% of Cd, the sharp peak was appeared at 435 nm which showed the induced optical mechanism in the molecular site. At 1.0 Wt.%, the

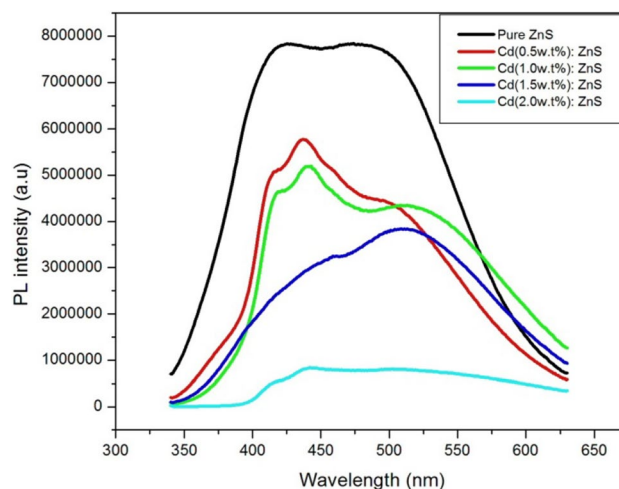


Fig. 7 PL spectra of pure and Cd doped ZnS nanoparticles at different doping concentrations nanoparticles

crest was observed at 442 nm which was 7 nm shifted than previous case. At 1.5 Wt.%, the well broad peak was found at 520 nm which was more shifted than 0.5 and 1.0 Wt.% samples [31–33]. Here, the peak was shifted to the higher wavelength region when the concentration of Cd increased. In the case of pure ZnS, the broad peak was incredibly observed as a broad one whereas at 2.0 Wt.%, the emission peak was found to be flat. From this observation; it was clear that, in pure ZnS, the cluster of electronic excitations taking place which was not controlled by the material itself. At minimum concentration of impurity (0.5 Wt.%), the electronic excitation was induced of excited degenerate orbitals which was customized by doping of Cd and the corresponding emission peak was appeared to be sharp and located at blue region [34]. At moderate concentration of Cd, the observed peak was rather shifted to the higher wavelength which was due to the inducement of optical catalytic process by impurity. At 1.5 Wt.%, the mechanism was further induced by the donating electrons by Cd impurity and the degenerate orbital's become more and thereby the

Table 3 Tentative vibrational assignments of ZnS nanoparticles

Vibrational assignments (cm^{-1})	Experimental absorption (cm^{-1})				
	Pure	0.5 wt.% Cd	1.0 wt.% Cd	1.5 wt.% Cd	2.0 wt.% Cd
O–H stretching	3257	2998	2920	2930	2930
C–H stretching	2355	2344	2359	2359	2341
CO_2 molecules	2181	2184	1618	1628	2039
	2060	2050	2042	2048	
O–H bending	1393	1385	1377	1383	1369
Carboxyl and methylene groups	1116	1126	1126	1116	1116
Zn–S stretching	798	809	817	817	817
Cubic ZnS	614	644	583	590	415

cluster of electronic emission taking place and the observed peak become broad [35, 36]. At 2.0 Wt.%, the line was flat which was due to that, no optical induced mechanism was found. Here, in all cases, the optoelectronic energized electron cloud was supplied by the doping impurity and it was restricted from 0.5 Wt.% to 1.5 and there was no inducement observed at 2.0 Wt.% of Cd.

3.5 Morphological characterization

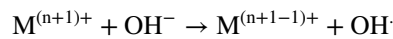
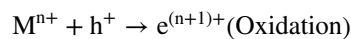
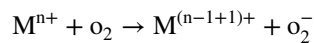
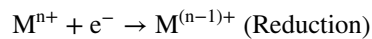
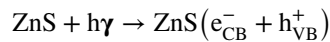
Nanoparticles analysis using SEM supplemented with EDX is carried out for the cubic ZnS to establish the morphology, grain size, shape and to confirm their chemical composition. SEM is well-known mesopores with large area pure and Cd doped ZnS nanoparticles and this is shown in Fig. 8 i & ii (a). These microscopes confirm that nanoparticles are grown in very high density. A closer study of these pictures reveal the orbital composition of a well-defined particles, which has spherical shapes. The EDX analysis Fig. 8b of pure ZnS clearly shows that the presence of elements such as, Zn and S indicate that the ZnS is composed of zinc and sulfide only. Cd doped ZnS (Fig. 8ii b) shows the occurrence of elements Cd along with Zn and S. The strong X-ray peaks associated with Zn K α , S K α and Cd K α in these spectrum. The atomic and weight percentages of Cd doped ZnS nanoparticles are shown in Table 5. The atomic and weight percentages Zn, S and Cd 39.94 at%, 24.06 wt%, 57.59at%, 70.73 wt% 2.47 at% and 5.21 wt%, respectively.

3.6 Transmission electron microscopy (TEM)

Direct measurements such as, TEM are essential to the precision particle size and nanomaterials. The typical image and selected area electron diffraction (SAED) patterns of pure and Cd doped ZnS nanoparticles are shown in Fig. 9. The particle size in pure ZnS is 3.68 nm and Cd doped ZnS is 3.6 nm, the particle size decreases in case of Cd doping as shown in Fig. 9 A1 and B1. The shape of the particle is spherical and it is shown in Fig. 9 A2 and B2. The SAED pattern corresponds to reflections of three strong crystal planes, which indicate (111) (220) and (311) and they are well alienated and evidenced with a tiny number of agglomeration [37]. No other diffraction rings are observed in the SAED patterns and it confirms that the cubic ZnS in the main phase is in superior agreement with the XRD results and it is shown in Figure A3. The diffraction rings are elongated to Cd doped into the ZnS nanoparticles and it is shown in Figure B3. The lattice fringes of ZnS nanoparticles are shown in Fig. 9 A4 with the width of the 0.35 nm. Figure B4 shows Cd doped ZnS nanoparticles width is 0.32 nm in lattice fringes. The width of the fringes has decrease in Cd doped ZnS nanoparticles.

3.7 Photocatalytic activity

The entanglement of the contribution of transition metal dopant ion are contributed in all of these processes. The photocatalytic mechanism is shown in Fig. 10. Performing as electron and/or hole traps is the most important function of dopant. The trap of charge carriers can decrease the recombination rate of electron–hole pairs but increase their life time. The process of charge trapping is as follows:



where M is the transition metal (Cd) ion dopant and n is the vacancy of the dopant ion. The energy level lies below the conduction band edge and the energy level of lies below the valance band edge. Thus the energy level of Cd metal ion infect the trapping efficiency. The photodegradation actually originated from the hydroxyl ($\cdot\text{OH}$) and superoxide anions (O_2^-) radicals result from the formation of (e^-/h^+) pairs in semiconductors [38]. As the catalyst exterior is photo-excited, the formation of electrons in conduction bands (e^-) and holes in valance bands (h^+) lead to transfer of charges on the photocatalyst sites. Its particular morphology increases the adsorption process of dye molecules on the exterior of the catalyst. These adsorbed dye molecules on the active sites of the semiconductor surface harvest the electrons in the conduction band of photocatalysts, leading to the formation of radical anions from the dyes and the degradation of the dye [39, 40]. ZnS nanoparticles with large surface area positively enhance the reaction due to the high adsorption of MO. The absorbance of MO solution is measured in ZnS nanoparticles at 268 nm and 464 nm, which corresponds to its maximum absorption wavelength. The degradation percentage (%D) of the MO dye can be considered from the subsequent equation,

$$\% D = \frac{C_0 - C_t}{C_0} \times 100$$

where % D is the Degradation percentage, C_0 is the Initial Concentration and C_t is the Concentration of dye is irradiated for selected time intervals (0–75 min). Figure 9 shows the absorption spectra of MO using ZnS catalyst as a function of wavelength (200–800 nm) for various time intervals 0, 15, 30, 45, 60, and 75 min. The degradation effect is characterized by monitoring the absorption peak of MO centered 268 nm and 464 nm. The plots directly exhibit that the

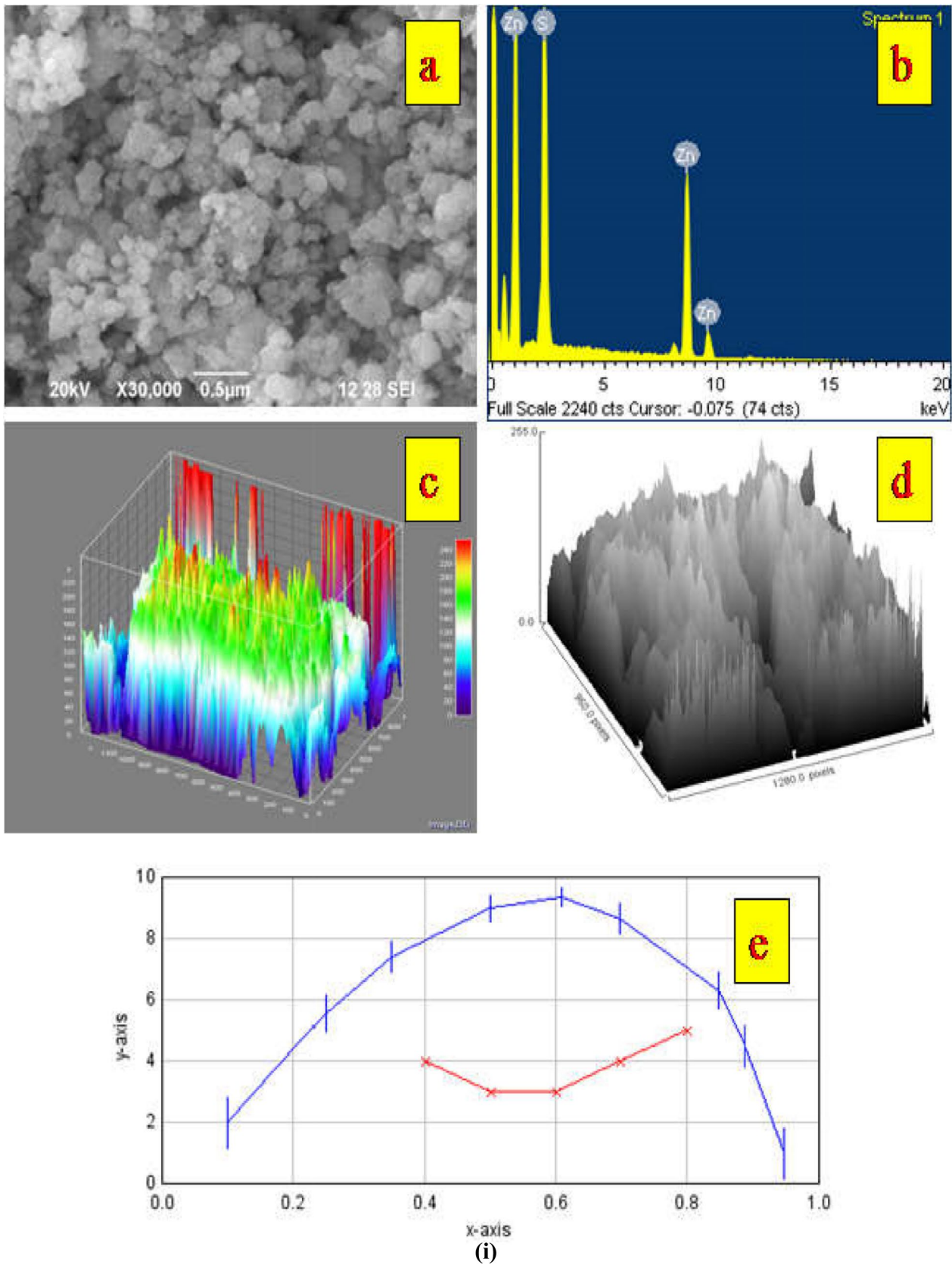


Fig. 8 (i) **a**, SEM image **a** pure, **b** EDX spectrum and **c–e** Surface Occupancy Plot (SOP) ZnS nanoparticles 8 (ii) (a), SEM image **a** 1.0 wt % Cd doped ZnS, **b** EDX spectrum and **c–e**, Surface Occupancy Plot (SOP) ZnS nanoparticles

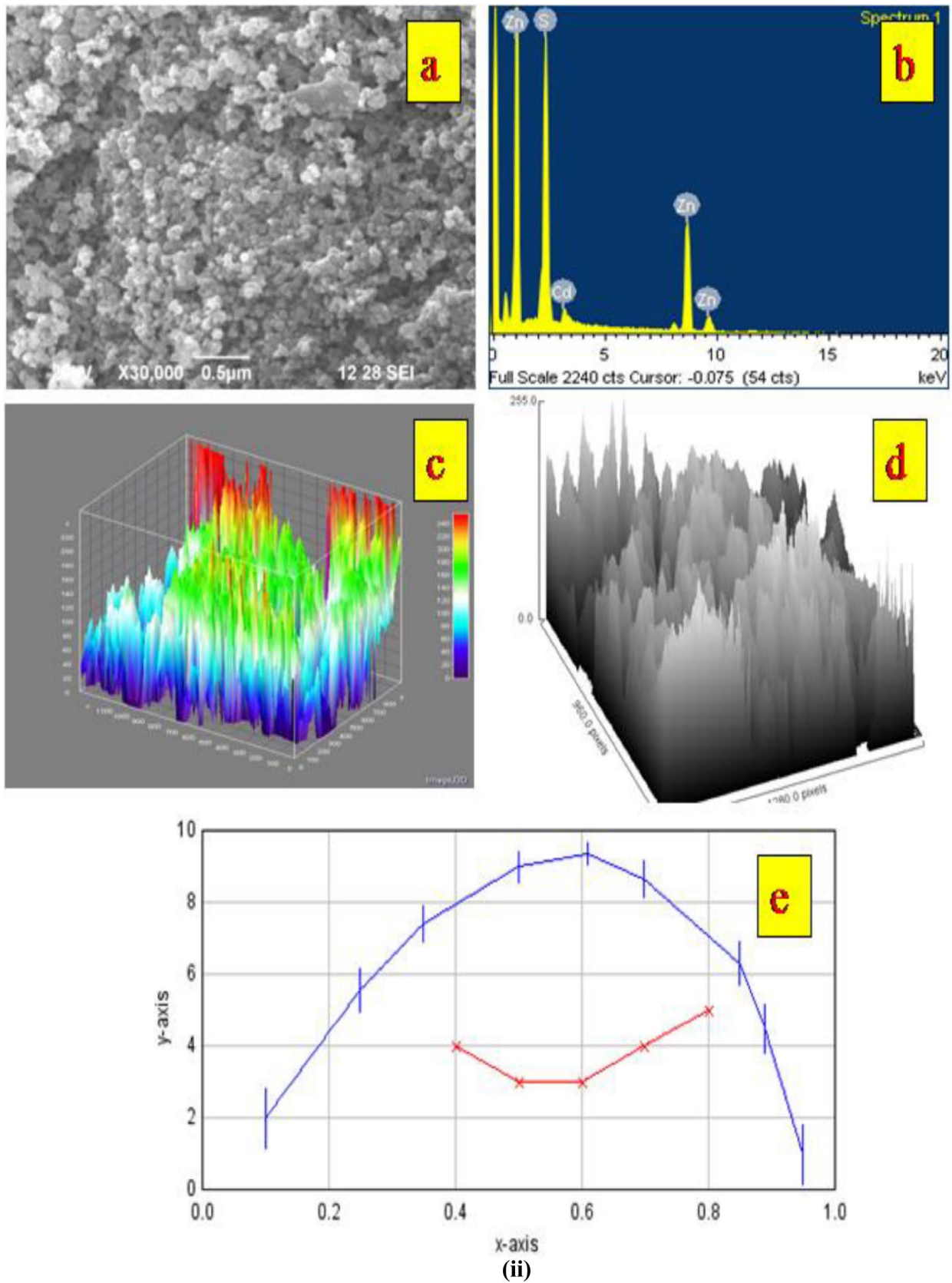


Fig. 8 (continued)

Table 4 Optical band gap of Pure and Cd doped ZnS nanoparticles

Sample	Bandgap (eV)
ZnS	3.66
(Cd0.5 wt.%) ZnS	3.54
(Cd1.0 wt.%) ZnS	3.70
(Cd1.5 wt.%) ZnS	3.77
(Cd2.0 wt.%) ZnS	3.45

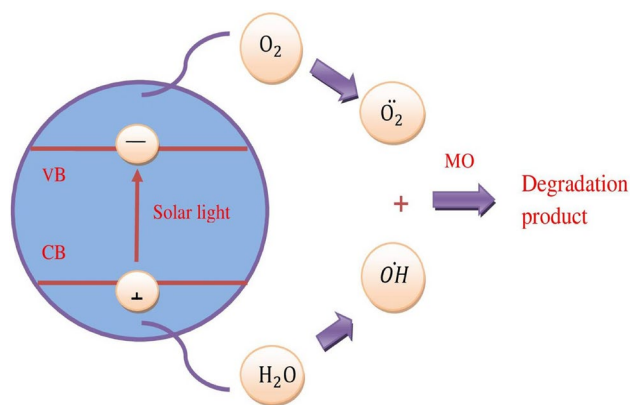
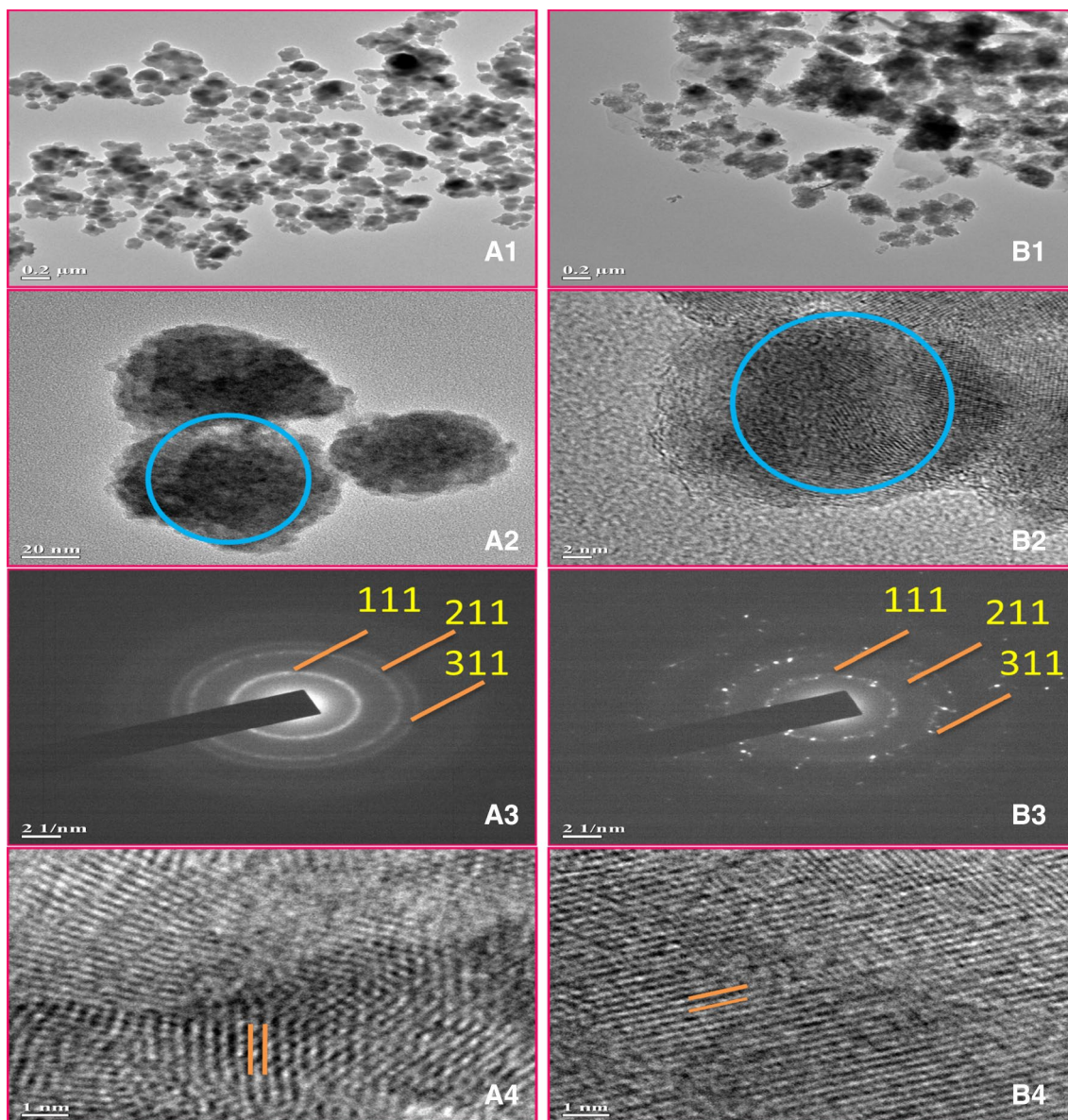
**Fig. 10** Mechanism of photocatalyst**Fig. 9** TEM images of ZnS nanoparticles (A1–B2), corresponding SAED pattern (A3–B3) and fringe pattern (A4–B4) of pure and Cd doped ZnS nanoparticles

Table 5 Elemental composition of Cd doped ZnS nanoparticles (reperused sample)

Element	Weight%	Atomic %
Zn	24.06	39.94
S	70.73	57.59
Cd	5.21	2.47
Total	100	100

maximum absorption peak decreases with increasing irradiation time. The effect of ZnS and Cd doped ZnS catalyst synthesized at degradation of the MO dye has been investigated by varying the time intermission from 0 to 75 min and the results obtained are in Table 6.

3.8 Kinetic of photocatlytic degradations

It is understood that the degradation of organic dyes by photo catalysts mainly follows pseudo first-order kinetics [41]

$$\ln \left(\frac{C_0}{C_t} \right) = kKt = kt$$

Or

$$C_0 = C_0 e^{-kt}$$

where k is the reaction rate constant and K is the adsorption co-efficient of the reactant. A plot of $\ln(C_0/C_t)$ versus time Fig. 11. Relation curve between $\ln(C_0/C_t)$ and time (t) represents a straight line; the slope equals the apparent

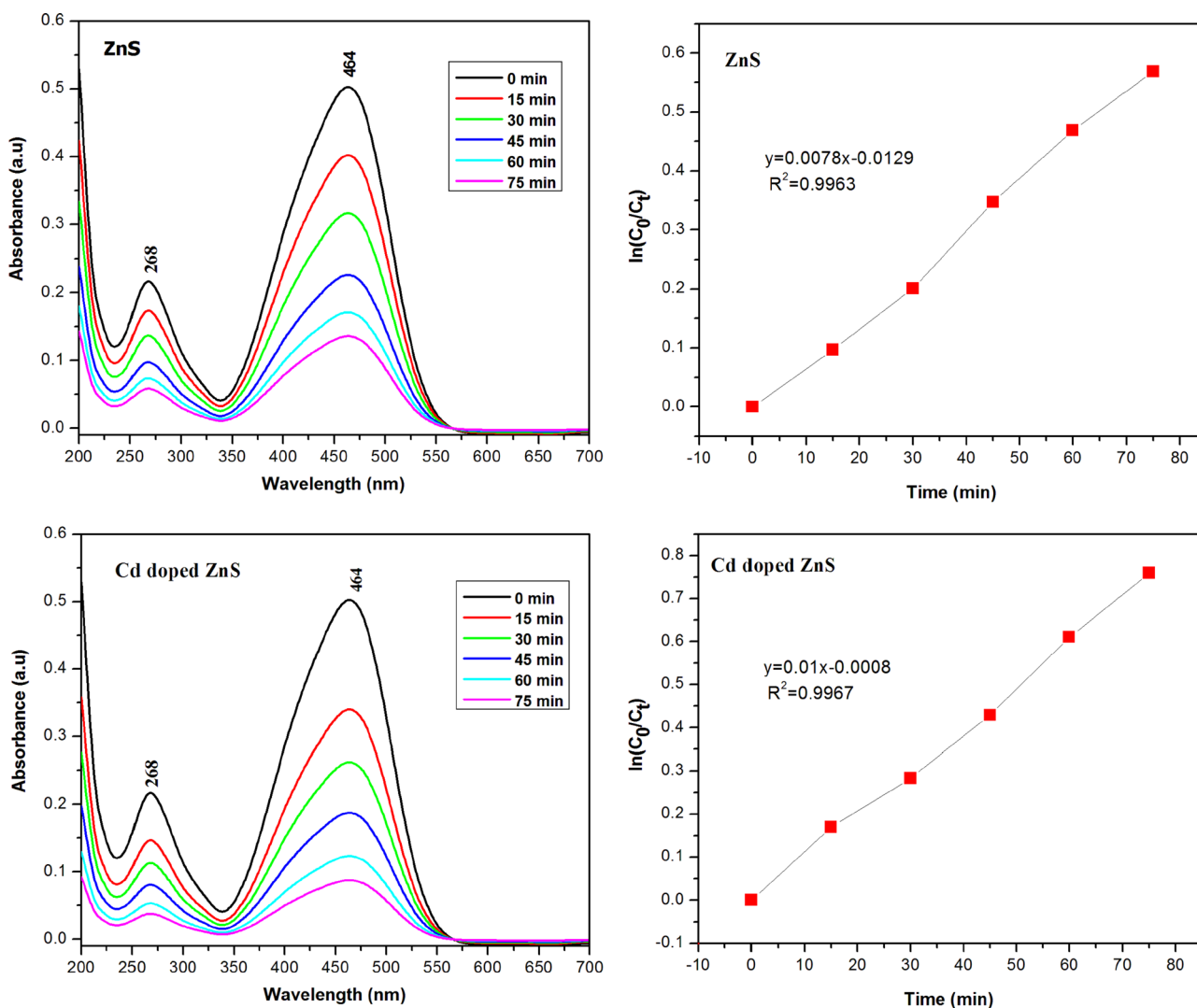


Fig. 11 UV–Vis absorption spectra of MO with respect to irradiation time versus Rate constant (k) and regression (R^2) for the Pure and Cd doped ZnS nanoparticles

Table 6 The effect of methyl orange (MO) dye degradation by Pure and Cd doped ZnS photocatalysts

Time (min)	% degradation of MO dye	
	ZnS	Cd doped ZnS
0	0	0
15	20	35.55
30	36.99	53.83
45	55.00	69.74
60	66.99	78.46
75	73.98	88.58

Table 7 Values of apparent rate constants k (min^{-1}) and regression for the degradation of 10 mM MO in the presence of Pure and Cd doped ZnS nanoparticles

Samples	Rate constants (min^{-1})	R^2
Pure ZnS	0.0078	0.9963
Cd doped ZnS	0.012	0.9967

first-order rate constant k . The kinetics of photodegradation of MO dye by ZnS nanoparticles are studied and the results are shown in Fig. 11. According to the pseudo-first-order rate equation, the rate constant (k) for MO degradation by ZnS nanoparticles are determined. The plot of $\ln(C_0/C_t)$ as a function of irradiation time gives the rate constant value 0.0078 min^{-1} . Moreover, the fitting correlation coefficient (R^2) is also determined to be 0.9963. Cd doped ZnS has rate constant value 0.01 min^{-1} and fitting correlation coefficient (R^2) is determined as 0.9967 and it is shown in Table 7.

3.9 Scavenger test

In order to know the reactive species responsible for MO dye degradation scavenger test were conducted with DMSO, P-BQ, and IPA for electron superoxide radical and hydroxyl radical respectively. To perform this experiment a mixture of 25 ml of 15 ppm MO, 0.03 Cd doped ZnS and 5 mM of scavenger solution was exposed to visible light for 30 min stirring condition. The above mixture was kept in dark 30 min to develop absorption–desorption equilibrium. From the above test it is concluded that super oxide radical play a major role in the photocatalytic reactive of dye.

4 Conclusions

The Pure and Cd doped ZnS nanoparticles with different doping concentrations at optimized temperature were effectively synthesized by solid state reaction method. The XRD

results exposed that the particles were along the direction (111) plane and showed the evidence of cubic type crystal structure. The optical band gap energy was increased with the increasing doping concentrations. The PL studies showed the existence of sulphur and zinc vacancies in Cd doped ZnS nanoparticles. The SEM and TEM photographs showed spherical shape morphology. The photocatalytic activity of prepared optimized Pure and doped sample was studied on degradation of Methyl orange (MO) dye. It was found that cubic phase showed tremendous photocatalytic activity on Methyl orange (MO) dye degradation. This photocatalytic degradation of MO was optimized to obtain higher degradation rate. This study concludes that the Cd doped ZnS nanoparticles are the promising photocatalyst on degradation of methyl orange dye.

References

1. S.K. Mishra, R.K. Srivastava, S.G. Prakash, R.S. Yadav, A.C. Pandey, Structural, optical and photoconductivity characteristics of mangeded doped cadmium sulfide nanoparticles synthesized by co-precipitation method. *J. Alloys Compd.* **513**, 118–124 (2012)
2. N.G. Iman, M.B. Mohamed, Optical properties of diluted magnetic semiconductor Cu: ZnS quantum dots. *Superlattice microstruct* **73**, 203–213 (2014)
3. W.T. Yao, S.H. Yu, S.J. Liu, J.P. Chen, X.M. Liu, F.Q. Li, Architectural control synthesis of CdS and CdSe nanoflowers, branched nanowires and nanotrees via a solvothermal approach in a mixed solution and then photocatalytic property. *J. Phys. Chem. B* **110**, (2006)11704–11710
4. Y.S. Xu, W.D. Zhang, Monodispersed Ag_3PO_4 nanocrystals loaded on the surface of spherical Bi_2MoO_6 with enhanced photocatalytic performance. *Dalton Trans.* **42**, 1094–1101 (2012)
5. Y.B. Liu, J.H. Li, B.X. Zhou, S.B. Lv, X.J. Li, H.C. Chen, Q.P. Chen, W.M. Cai, Photoelectrocatalytic degradation of refractory organic compounds enhanced by a photocatalytic fuel cell. *Appl. Catal. B* **111–112** (2012) 485–491
6. P. Sathishkumar, R.V. Mangalaraja, S. Anandan, M. Shokkumar, $\text{CoFe}_2\text{O}_4/\text{TiO}_2$ nanocatalysts for the photocatalytic degradation of Reactive Red 120 in aqueous solutions in the presence and absence of electron acceptors. *Chem. Eng. J.* **220**, 302–310 (2013)
7. Y.B. Liu, J.H. Li, B.X. Zhou, H.C. Chen, Z.S. Wang, W.M. Cai, TiO_2 -nanotube array-based photocatalytic fuel cell using refractory organic compounds as substrates for electricity generation. *Chem. Commun.* **47**, 10314–10316 (2011)
8. J.B. Joo, Q. Zhang, I. Lee, M. Dahl, F. Zaera, Y.D. Yin, Mesoporous anatase titania hollow nanostructures through silica-protected calcination. *Adv. Funct. Mater.* **22**, 166–174 (2012)
9. Y.H. Xiao, L.Z. Lu, A.Q. Zhang, Y.H. Zhang, L. Sun, L. Huo, F. Li, Highly enhanced acetone sensing performances of porous and single crystalline ZnO nanosheets: high percentage of exposed (100) facets working together with surface modification with Pd nanoparticles. *ACS Appl. Mater. Interfaces* **43**, 797–3804 (2012)
10. A. Fujishima, K. Honda, Electrochemical photolysis of Water at a semiconductor electrode. *Nature* **238**, 37–38 (1972)
11. T. Inoue, A. Fujishima, S. Konishi, K. Honda, Photoelectrocatalytic reduction of carbon dioxide in aqueous suspensions of semiconductor powders. *Nature* **277**, 637–638 (1979)
12. X. Xiang, L.S. Xie, Z.W. Li, F. Li, Ternary $\text{MgO}/\text{ZnO}/\text{In}_2\text{O}_3$ heterostructured photocatalysts derived from a layered precursor and

- visible-light-induced photocatalytic activity. *Chem. Eng. J.* **221**, 222–229 (2013)
13. Z.C. Wang, J.H. Liu, W. Chen, Plasmonic Ag/AgBr nanohybrid: synergistic effect of SPR with photographic sensitivity for enhanced photocatalytic activity and stability. *Dalton Trans.* **41**, 4866 (2012)
 14. A.K. Kole, S. Gupta, P. Kumphakar, P.C. Ramamurthy, Nonlinear optical second harmonic generation in ZnS quantum dots and observation on optical properties of ZnS /PMMA nanocomposites. *Opt. Commun.* **313**, 231–237 (2014)
 15. M. Navaneethan, J. Archana, K.D. Nisha, Y. Hayakawa, S. Pon-nusamy, C. Muthamizhchelvan, Temperature dependence of morphology, structural and optical properties of ZnS nanostructures synthesized by wet chemical rout. *J. Alloys compd* **506**, 249–252 (2010)
 16. H. Ali, S. Karim, M.A. Rafiq, K. Maaz, A. urRahman, A. Nisar, M. Ahmad, Electrical conduction mechanism in ZnS nanoparticles. *J. Alloy. Compd.* **612**, 64–68 (2014)
 17. L. Dong, Y. Chu, Y. Zhang, Microemulsion-mediated solvothermal synthesis of ZnS nanowires. *Mater. Lett.* **61**, 4651–4654 (2007)
 18. J. Zhao, R. Liu, Surfactant-free hydrothermal synthesis and optical properties of ZnS solid microspheres. *Mater. Lett.* **124**, 239–241 (2014)
 19. P.K. Ghosh, U.N. Maiti, S. Jana, K.K. Chattopadhyay, Field emission from ZnS nanorods synthesized by radio frequency magnetron sputtering technique. *Appl. Surf. Sci.* **253**, 1544–1550 (2006)
 20. W. Zhang, X. Zeng, H. Liu, J. Lu, Synthesis and investigation of blue and green emission of ZnS ceramics, *Lumin.* **134**, (2013)498–503
 21. L.P. Wang, G.Y. Hong, A new preparation of Zinc Sulfide nanoparticles by solid state method at low temperature. *Mater. Res. Bull.* **35**, 695–701 (2000)
 22. Z. Deng, H. Yan, Y. Liu, Controlled colloidal growth of ultrathin single-crystal ZnS nanowires with a magic size diameter. *Angew. Chem. Int. ed* **49**, 8695–8698 (2010)
 23. G. Kiruthigaa, C. Manoharan, C. Raju, J. Jayabharathi, S. Dhanapandian, Solid state synthesis and spectral investigations of nanostructure SnS^2 . *Spectrochimica Acta Part A* **129**, 415–420 (2014)
 24. R. Sridhar, C. Manoharan, S. Ramalingam, S. Dhanapandian, M. Bououdina, Spectroscopic study and optical and electrical properties of Ti-doped ZnO thin films by spray pyrolysis. *Spectrochimica Acta Part A* **120**, 297–303 (2014)
 25. G. Murugadoss, M.R. Kumar, Synthesis and optical properties of monodispersed Ni^{2+} doped ZnS nanoparticles. *Appl. Nanosci.* **4**, 67–75 (2014)
 26. M. Jothibas, C. Manoharan, S.J. Jeyakumar, P. Praveen, I.K. Punithavathy, J.P. Richard, Synthesis and enhanced photocatalytic property of Ni doped ZnS Nanoparticles. *Sol. Energy* **159**, 434–443 (2018)
 27. M.A. Hines, P. Guyot-sionnest, Synthesis and characterization of strongly luminescing ZnS-Capped CdSe nanocrystals. *J. Phys. Chem.* **100**, 468–471 (1996)
 28. R. Viswanatha, S. Sapra, S.S. Gupta, Synthesis and characterization of Mn doped ZnO nanocrystals, *J. Phys. Chem. B*, 108:192–198, no.20, pp. 6303–6310, 2004
 29. Y.V.B. de Santana, C.W. Raubach, M.M. Ferrer, F. La Porta, J.R. Sambrano, V.M. Longo, E.R. Leitie, E. Longo, Experimental and theoretical studies on the enhanced photoluminescence activity of Zinc Sulfide with a capping agent. *J. Appl. Phys.* **110**, 123507–112315 (2011)
 30. F.A. La Porta, M.M. Ferrer, Y.V.B. de Santan, C.W. Raubach, V.M. Longo, J.R. Sambrano, E. Longo, J. Andrés, M.S. Lie, J. Varela, Towards an understanding on the role of precursor in the synthesis of ZnS nanostructures. *J. Alloys Curr. Phys. Chem.* **3**, 378–385 (2013)
 31. S.S. Kumar, M.A. Khadar, S.K. Dhara, T.R. Ravindran, K.G.M. Nair, Photoluminescence and Raman studies of ZnS nanoparticles implanted with Cu + ions. *Nucl. Instrum. Meth. B* **251**, 435 (2004)
 32. P.H. Borse, N. Deshmukh, R.F. Shinde, S.K. Date, S.K. Kulkarni, Luminescence quenching in ZnS nanoparticles due to Fe and Ni doping. *J. Mater. Sci.* **34**, 6087–6093 (1999)
 33. H.Y. Lu, S.Y. Chu, S.S. Tan, The characteristics of low-temperature-synthesized ZnS and ZnO nanoparticles. *J. Cryst. Growth* **269**, 385 (2004)
 34. P. Kaur, S. Kumar, C.L. Chen, K.S. Yang, D.H. Wei, C.L. Dong, C. Srivastava, S.M. Rao, Gd doping induced weak ferromagnetic ordering in ZnS nanoparticles synthesized by low temperature coprecipitation technique. *Mater. Chem. Phys.* **186**, 124–130 (2016)
 35. G.S. Lotey, Z. Jindal, V. Singhi, N.K. Verma, Structural and photoluminescence properties of Eu doped ZnS nanoparticles. *Mater. Sci. Semicond. Process.* **16**, 2044–2050 (2013)
 36. S. Biswas, S. Kar, S. Chaudhuri, Optical and magnetic properties of manganese incorporated zinc sulfide nanorods synthesized by a solvothermal process. *J. Phys. Chem. B* **109**, 17526–17530 (2005)
 37. V.D. Mote, Y. Purushotham, B. N. Dole, Structural, morphological and optical properties of Mn doped ZnS nanocrystals. *Ceramica* **59**, 614–619 (2013)
 38. Q. Xiang, J. Yu, M. Jaroniec, Graphene-based semiconductor photocatalysts. *Chem. Soc. Rev.* **41**, 82–796 (2012)
 39. X. Zhao, L. Wang, X. Xu, X. Lei, S. Xu, F. Zhang, Fabrication and photocatalytic properties of novel $\text{ZnO}/\text{ZnAl}_2\text{O}_4$ nanocomposite with ZnAl_2O_4 dispersed inside ZnO network. *AICHE J.* **58**, 573–582 (2012)
 40. N. Sapawe, A. Jalil, S. Triwahyono, One-pot electro-synthesis of $\text{ZrO}_2\text{-ZnO}/\text{HY}$ nanocomposite for photocatalytic decolorization of various dye contaminants. *Chem. Eng. J.* **225**, 254–265 (2013)
 41. C.L. Yu, F.F. Cao, X. Li, G. Li, Y. Xie, J.C. Yu, Q. Shu, Q.Z. Fan, J.C. Chen, Hydrothermal synthesis and characterization of novel PbWO_4 microspheres with hierarchical nanostructures and enhanced photocatalytic performance in dye degradation. *Chem. Eng. J.* **219**, 86–95 (2013)

Publisher's Note Springer Nature remains neutral with regard to jurisdictional claims in published maps and institutional affiliations.